



Direct conversion of carbon nanofibers and nanotubes into diamond nanofibers and subsequent growth of large-size diamonds

Journal:	<i>Nanoscale</i>
Manuscript ID	NR-ART-11-2018-008823.R2
Article Type:	Paper
Date Submitted by the Author:	14-Dec-2018
Complete List of Authors:	<p>Narayan, Jagdish; North Carolina State University , Materials Science and Engineering Bhaumik, Anagh; North Carolina State University, Department of Materials Science and Engineering Sachan, Ritesh; North Carolina State University , Materials Science and Engineering; US Army Research Office, Materials Science Division Haque, Ariful; North Carolina State University , Materials Science and Engineering Gupta, Siddharth; North Carolina State University , Materials Science and Engineering Pant, Punam; North Carolina State University , Materials Science and Engineering</p>

Direct conversion of carbon nanofibers and nanotubes into diamond nanofibers and subsequent growth of large-size diamonds

J. Narayan,^{1*} A. Bhaumik,¹ R. Sachan,^{1,2} A. Haque,¹ S. Gupta,¹ and P. Pant¹

¹Department of Materials Science and Engineering, Centennial Campus, North Carolina State University, Raleigh, NC 27695-7907, USA

² Materials Science Division, Army Research Office, Research Triangle Park, NC 27709, USA

*Correspondence to: narayan@ncsu.edu

Abstract

We report a pulsed laser annealing method to convert carbon fibers and nanotubes into diamond fibers at ambient temperature and pressure in air. The conversion of carbon nanofibers and nanotubes into diamond nanofibers involves melting in a super undercooled state using nanosecond laser pulses, and quenching rapidly to convert into phase-pure diamond. The conversion process occurs at ambient temperature and pressure, and can be carried out in air. The structure of diamond fibers has been confirmed by selected-area electron diffraction in transmission electron microscopy, electron-back-scatter-diffraction in high-resolution scanning electron microscopy, all showing characteristic diffraction lines for diamond structure. The bonding characteristics were determined by Raman spectroscopy with a strong peak at near 1332 cm^{-1} , and high-resolution electron- energy-loss spectroscopy in transmission electron microscopy with a characteristic peak at 292 eV for σ^* for sp^3 bonding and absence of π^* for sp^2 bonding. The Raman peak at 1332 cm^{-1} downshifts to 1321 cm^{-1} for diamond nanofibers due to the phonon confinement in nanodiamonds. These laser-treated carbon fibers with diamond seeds are used to grow larger diamond crystallites further by using standard hot-filament chemical vapor

deposition (HFCVD). We compare these results with those obtained without laser treating the carbon fibers. The details of diamond conversion and HFCVD growth are presented in this paper.

1. Introduction:

Direct conversion of carbon into diamond has fascinated scientists from all over the world for the longest time, because it is thermodynamically challenging with many exciting technological applications ranging from quantum computing, sensing and communication to field emission and tool coatings for oil and gas exploration and deep-sea drilling, in addition to diamond jewelry.^{1,2} According to the thermodynamic equilibrium phase diagram, carbon/graphite can be converted into diamond at high temperature (5000K) and pressure (12GPa). These pressures and temperatures are somewhat reduced in the presence of catalysts. That is how diamond grits are produced industrially and the Nature accomplishes this naturally in the Earth's crust.³ For polycrystalline graphitic rods, lower temperatures (2573-2723K) for diamond conversion at higher pressures (12-25GPa) have been reported.⁴

Recently, we reported a major breakthrough in the conversion of carbon thin films into diamond by overcoming thermodynamic constraints with the help of kinetics.^{5,6} By using high-power nanosecond laser pulses, amorphous carbon layers were melted in a highly undercooled state and quenched subsequently into phase-pure diamond or into a new phase of Q-carbon at a higher undercooling. Remarkably, parallel results were obtained for the conversion of h-BN into c-BN or Q-BN.⁷ These diamond and c-BN structures were doped with *n*- and *p*-type dopants with concentrations far higher than equilibrium thermodynamic solubility limits as a result of rapid quenching from liquid and solute trapping phenomenon. We were able to control nature and number density of defects in diamond and c-BN more precisely from liquid phase growth, which is an important consideration for solid-state devices, as the annealing of as-grown defects in these materials require annealing temperatures exceeding 1700°C.⁷

These diamond structures can be used as seed precursors to grow large-size diamond structures by hot-filament chemical vapor deposition (HFCVD) and microwave-plasma chemical vapor deposition (PECVD). The HFCVD and PECVD require seeding on which CH_x species are attached during diamond growth. Carbide forming substrates provide these nucleation sites. In the case of noncarbide forming substrates, strain centers and surface roughening by scratching and pulsed laser annealing can provide some diamond nucleation sites. One-dimensional structures of diamond with size ranging from nano to micrometers will play a crucial role for nanoscale devices with new functionalities, ranging from quantum computing, sensing and communication to efficient catalysts and field emission displays. Conversion of carbon tubes and fibers into diamond fibers/rods provides a direct access to these devices. Diamond nanorods (DNRs) in the form of pillars have been created from polycrystalline⁸ and single-crystal diamond films⁹ by using microwave plasma and reactive ion etching methods. Other extensive research efforts in this area have focused on direct formation of DNRs using CVD (chemical vapor deposition) methods and direct conversion of carbon into diamond. This is a very expensive and cumbersome process with a limited yield of polycrystalline structures. The CVD based methods require atomic hydrogen and carbon containing species. Formation of DNRs with 4-8 nm and ~100nm length) was reported by Sun *et al* after prolonged (>20h) hydrogen plasma treatment of carbon nanotubes at 1000K.¹⁰ Hsu *et al* reported the synthesis of DNRs by chemical vapor deposition at ambient pressure by introducing during CNT growth process.¹¹ In both of these cases, nanotubes provide the source for carbon containing CH_x species and nucleation sites for diamond growth. These methods produce diamond mixed with amorphous carbon with limited yield, and involve toxic gases at high temperatures.

In the area of direct conversion, Wei *et al.* reported the conversion of carbon nanotubes into diamond through the formation of carbon onion phase via solid-phase transformation.¹² The process involved coating of the carbon nanotubes on a cast iron substrate, followed by CO₂ CW laser irradiation. Luo *et al* reported the formation of diamond nanocrystals at the tips of carbon nanofibers after spark plasma sintering (SPS) at 1500⁰C and atmospheric pressure, and explained it *via* the formation by an intermediate phase of carbon onion.¹³ Zhang *et al* found the conversion of tips of multi-walled carbon nanotubes (MCNTs) into diamond after SPS at 1200⁰C and explained by nanotube to carbon onion to diamond process.¹⁴ Ozden *et al* showed that ballistic fracturing of CNTs can lead to formation of nanodiamonds,¹⁵ which is consistent with transformation of carbon nanotubes into diamond at high pressures and temperatures (4.5 GPa at 1300⁰C).¹⁶ More recently, J. Zhang *et al* showed the conversion of carbon nanotubes into T-carbon by using pico-second laser irradiation.¹⁷ Perez del Pino *et al.*¹⁸ reported the formation of different forms of amorphous carbon, including nanodiamonds by using pulsed laser irradiation (266 nm NdYAG laser with 3 ns pulse duration and 40-100 mJcm⁻²) of MWCNTs in nitrogen atmosphere. However, characteristic Raman (near 1332 cm⁻¹) and EELS (at 292 eV) peaks for the diamond phase were not observed. The TEM fringe contrast, which is not very reliable, is reported for [200] and [100] orientation. They meant for (200) and (110) planes, which are not the diffracting planes of diamond. Normally, (111) planes should be present with cross-fringes for reliability based upon two sets of {111} planes. It is envisaged that there is not enough undercooling due to very short laser pulses, which is the key to the formation of diamond phase.⁵ It should be noted that none of these previous methods invoked melting and undercooling as the mechanism for conversion of carbon-based structure into diamond.

Here we report the conversion of carbon fibers (available inexpensively) and nanotubes into diamond fibers by nanosecond pulsed laser melting. In our previous work based on laser induced diamond conversion, we have shown that undercooling plays an important role.⁵ The sapphire, plastic, and glass substrates provide sufficient undercooling in the case of amorphous thin films of carbon. In the present case, the restriction of heat flow (1D) in CNT/CNF provides enough undercooling to cause the conversion. The melting in the middle of CNT/CNF leads to formation of sp^3 enriched amorphous carbon as a result of rapid heat flow and less undercooling. We have carried out detailed laser-solid interaction simulations to determine optimized conditions for undercooling and conversion into diamond or a new phase of carbon, namely Q-carbon.⁵ The formation of beads at the tips of nanofibers and nanotubes provides a direct evidence for the melting process. The conversion process starts at the tips and bends, which can be extended with the number of pulses to cover entire lengths. There is a critical diameter of the fiber below which there is a complete conversion into diamond. Above this critical size, diamond nanocrystallites are formed on the surface, some of which grow rapidly to form diamond nanorods normal to the substrate. These nanostructures are ideally suited for applications ranging from enhanced catalysis to field emission. We have used these laser-annealed fibers as seeds for further growth to obtain larger sizes and areas using conventional HFCVD (hot-filament chemical vapor deposition) and PECVD (plasma-enhanced chemical vapor deposition). We have compared these results from laser-annealed fibers with untreated carbon fibers, and found considerably enhanced diamond nucleation and growth in laser-annealed fibers.

2. Experimental:

The CNFs are synthesized in a tube furnace-CVD chamber thermally baked at 800°C. Highly sensitive mass flow controllers are used to introduce Ar (450 sccm) and H₂ (10 sccm) in the tube

furnace prior to the CVD processing. The temperature in the CVD furnace is ramped up to 800°C and thermally soaked for 10 min. At this temperature, 25 sccm of C₂H₄ is introduced in the furnace for 30 minutes. After that, the Ar and H₂ gases are flown in the tube furnace and the flow of C₂H₄ was switched off. The temperature is then ramped down to room temperature for 2 hours. The prepared CNFs are ultrasonicated to remove unwanted metallic impurities. These CNFs are irradiated in air with ArF laser pulses (pulse duration = 20ns, wavelength = 193nm, energy density = 0.6-1.0 Jcm⁻²). Due to the restriction of heat flow in one-dimensional CNFs, melting of amorphous carbon occurs leading to a highly undercooled state. The undercooled state is subsequently quenched to form nanostructures of diamond. With increasing the number of nanosecond laser pulses, the entire fibers are converted into diamond fibers (DNFs). The CNFs (before and after PLA processing) are dispersed in ethanol and transferred onto copper TEM grids. To facilitate the bleeding of electronic charges, the sample is sandwiched between two copper grids and then mounted in the TEM sample holder. The laser-annealed carbon fibers were used for seeding the diamond growth by HFCVD (hot-filament chemical vapor deposition with 2.0% CH₄ in H₂) at 1100K substrate temperature and filament temperature of 2300K. These structures are characterized by TEM, SAED, EBSD, SEM, and Raman spectroscopy (using 532 nm excitation laser). High-resolution SEM (and EDX) and EBSD (electron-scatter-back diffraction) measurements are carried out using FEI Verios 460L SEM and FEI Quanta 3D FEG FIB-SEM, respectively. The EBSD technique provides three-dimensional (Kikuchi) diffraction patterns for phase identification and structural morphology is determined by high-resolution SEM. The JEOL 2000 FX is used for performing the TEM and SAED of the CNFs and DNFs. A 200 kV electron beam from LaB₆ source (having point-to-point resolution of 0.14 nm) is used for the TEM imaging and diffraction. A HORIBA Xplora PLUS confocal Raman microscope

having 0.5 μm spatial resolution and 532 nm excitation source is used for determining the Raman active vibrational characteristics (at 300 K) of the CNFs and DNFs. The Raman spectroscopy provides a distinctive identification of diamond and related materials.

3. Results and discussion:

Figure 1 shows an SEM micrograph of pristine carbon nanofibers before pulsed laser annealing where the structure of carbon is amorphous and contains some surface roughness (Fig. 1a). This surface roughness increases with size or diameter of the nanofiber. After a single 20ns (193nm ArF) laser pulse at ambient temperature and pressure, we observed a direct conversion of carbon nanofiber into crystalline diamond (Fig. 1b). The conversion process starts at the tips and bends and is more efficient for thinner fibers (less than 50 nm diameter for this diameter. Fig. 1 (b) shows a comparison of the conversion of thin 35 nm diameter fiber, whereas 60nm diameter fiber shows formation of nanodiamonds only on the surface. The fiber orientation also plays an important role with more efficient conversion for fibers aligned along the beam. Fig. 2 shows a large number of carbon fibers after laser annealing with 10 laser pulses, where the effect of size (diameter) and orientation of fibers with respect to laser beam are clearly shown. The carbon fibers with diameter less than 50 nm diameter are converted fully into diamond, whereas larger diameter fibers show the formation of diamond on the surface. These diamond nuclei on the surface can grow normal to the carbon fiber during irradiation with subsequent pulses. From the length of the diamond fiber, the diamond growth velocities are estimated to be about 2 ms^{-1} , which is consistent with theoretical modeling presented below. These nanostructures are ideally suited for diamond based catalytic applications.

The crystal structure determination of as-grown DNFs was carried out by the electron beam scatter diffraction (EBSD) technique in the high-resolution SEM, as shown in Fig. 3. The

EBSD is a powerful non-destructive technique to determine the details of atomic structure of crystalline phases by providing three-dimensional diffraction (Kikuchi) patterns. The electron probe size used for EBSD is ~ 10 nm and thus it is ideal for determination of structure along the length of the diamond fiber. The EBSD results are shown as the inset in Fig. 3 from the encircled region near the tip of the fiber. The characteristic Kikuchi diffraction pattern of diamond and relative orientation are depicted in a red cube. There was a minimal change in the crystal orientation (Kikuchi diffraction pattern) along the length from the tip, as revealed by the EBSD patterns. The highest undercooling occurs at the tip and falls as we move more towards the base (of CNF). The amorphous nature of CNF was found to be unaltered close to its base. Figure 4(a) shows Raman results from carbon nanofibers before and after laser treatment. The Raman peak corresponding to nanodiamonds is observed ~ 1321 cm^{-1} in the CNF samples after the PLA processing. Figure 4(b) shows Raman spectra of CNT after PLA. The peak at 1324.2 cm^{-1} corresponds to diamond formed after the PLA. The downshift (from 1332 cm^{-1} in microdiamonds) and spectral broadening are due to phonon confinement¹⁸ in nanosized diamonds (formed after PLA). Therefore, Raman studies provide a clear and consistent evidence for conversion of CNFs into nanodiamonds (due to laser-assisted melting and resolidification) after the PLA treatment. Figure 5 depicts the TEM (transmission electron microscopy) and SAED (selected-area electron diffraction) analysis of carbon fibers after laser annealing. Fig. 5 (a) shows the formation of diamond near the tip of the carbon fibers. The SAED pattern covering many nanodiamond tips, which are oriented differently, is shown in Fig. 5(b). The SAED pattern shows characteristic diffraction pattern (diffraction rings) of nanocrystalline diamond showing the distinct diffractions peaks of 111, 200, 220, 311, 222, 004, 331, and 333 planes. We observe (200) diffraction ring in TEM due to multiple diffraction from two sets of (111) and (1-1-1)

planes. The diffraction from the base of the fiber contained characteristic amorphous structure, which is similar to that of unirradiated carbon. Figure 5(c) depicts SEM-EDX of the tip of DNF (formed after PLA). The EDX spectrum depicts the presence of only C-K α_1 peak at 0.277 keV (and no other impurity peaks). This shows that the phase transformation of amorphous CNF into diamond occurs in the absence of a catalyst (at room temperatures and atmospheric pressures). High-resolution electron- energy-loss spectroscopy in transmission electron microscopy showed a characteristic peak at 292 eV for σ^* for sp³ bonding and absence of π^* at 284 eV for sp² bonding.

Fig. 6 (a) shows a theoretical calculation of melt depth as function of time of carbon substrate. The carbon is found to melt in a highly undercooled state, and quenching from this state leads to the formation of diamond. The melting starts after 10ns of the incidence of the laser pulse, melt-in front rapidly penetrates up until the end of the laser pulse. After that solidification occurs with underlying seed. As shown in Figure the solidification velocity is of the order 2-5ms⁻¹. The temperature profile in Fig 6(b) shows that amorphous carbon melts ~4000K in a highly undercooled state, close to 1000K below the equilibrium melting of graphite. The pulsed laser annealing process is carried out in atmospheric pressure and room temperature (in air). No external heat is applied during the conversion. The temperature ~4000 K is attained after laser-material interaction, and this undercooled state results in the formation of diamond upon quenching. During the transformation of CNTs and CNFs, the temperature rises locally to 4000K, but it is for very short time often less than 100ns. As a result, overall temperature rise of the system is less 5K. These calculations were performed using SLIM Computer program using Melting temperature.¹⁹ The pulsed laser annealing of nanofibers leads to melting of carbon, and subsequent quenching from a highly undercooled state results in the direct conversion of carbon

into diamond. Our earlier studies on melting of amorphous carbon films on sapphire substrates have shown that molten carbon can be converted into diamond at an undercooling $\sim 1000\text{K}$, and into a new form of carbon (named Q-carbon) at a higher undercooling at ambient temperatures and pressures in air.

Fig. 7 shows conversion of carbon nanotubes into diamond nanofibers after 10 laser shots at 0.65 Jcm^{-2} of the ArF laser. The conversion process in the case of nanotubes is similar to that of nanofibers, as the conversion process starts from the tips and bends, and it is more efficient for both nanotubes and fibers which are aligned normal to the substrate. The diameter of carbon nanotubes ranged from 10-50nm (mostly double-walled) with over 300nm in length. Fig 7(a) shows a low-magnification SEM image, showing nanotubes of varying sizes with diamond formation near the tips. The diamond tips are considerably sharper due to smaller amount of carbon available in the hollow nanotubes. The details of diamond conversion near the tips are shown in Figs 7(b) and Fig. 7 (c), where nanodiamond beads are formed with a direct evidence of carbon melting during the conversion process. Fig. 7(d) shows the formation of nanodiamonds normal to the carbon nanotubes (marked with arrows). These results show the formation of sharpest diamond nanoneedles by this direct conversion of carbon nanotubes into diamond.

A detailed electron microscopic analysis is performed on the laser annealed CNTs, and the results are shown in Figure 8. A representative HAADF image of laser annealed CNTs is presented in Figure 8a, demonstrating the formation of nanodiamonds in various regions on CNTs. The average size of the nanodiamonds is estimated to be $\sim 3 \pm 1\text{ nm}$, while CNTs are measured to be $\sim 7 \pm 1\text{ nm}$ diameter. Figure 8b further shows the formation of nanodiamonds on an individual CNT, clearly showing the emergence of nanodiamond at the tip of the CNT. This supports the earlier proposed hypothesis of diamond formation through ultrafast melting and

non-equilibrium super undercooling of CNT. Various diamonds are also observed on the body of CNTs formed under similar conditions but through partial melting of CNTs. We have also performed the EELS at ~ 700 eV where no peaks of Fe are observed. SEM-EDX also shows no Fe content in the CNF/CNTs. In addition, the contrast in ADF image is primarily coming due to thickness and density of the material, as the density of diamond is ~ 3 times higher than that of CNTs. Using low-loss EELS, the relative thickness (long ratio) on diamond is estimated to be 0.80, while that on neighboring CNT region is 0.15. Electron energy-loss (EEL) spectra are also obtained from the nanodiamonds, CNT and nanodiamonds, and unannealed CNT are shown in figure 8(c), (d), and (e), respectively. The spectra are shown along with the reference CNT and diamond EEL spectra for a comparison. The EEL spectrum obtained from the nanodiamonds (figure 8(c)) exhibit the near edge fine structure peaks at 292, 297, 305, and 326 eV, which are broader than the typical reference spectrum from diamonds. The broadening in the characteristic peaks is attributed to the strained nature of nanodiamonds. The EELS in figure 8(c) is acquired from the region in converted nanodiamond where π^* peak is clearly absent. As shown in figure 8(d), EEL spectrum suggests diamond and CNT regions to be overlapping which is found very frequently during the analysis. The additional strong π^* (284 eV) peak is clearly observed in figure 8(d). The appearance of π^* peak is due to the presence of underneath CNT. The EEL spectrum obtained from CNT appears to be consistent with the typical reference spectra. It should be mentioned that under intense electron flux due to small probe-size during EELS, diamond was found to convert nanodiamonds into amorphous graphitic phase of carbon.

Fig. 9 (a) shows the formation of large diamond crystallites in HFCVD reactor after deposition for three hours by using the seeding of laser annealed diamond nanofibers. These crystallites have remarkably uniform size, where the average size of diamond crystallites was

determined to be 2.2 μm . This is consistent with average diamond nuclei of about 100nm with growth rate of about 700nm/hr. The 100 nm diamond nuclei from undercooled liquid carbon in 50ns with diamond growth rate of about 2 ms^{-1} . Fig. 9(b) shows diamond HFCVD growth on carbon nanofibers which were not treated with lasers. The number density of diamond crystallites is considerably higher for laser-annealed fibers (Fig. 9(a)) compared to untreated carbon fibers (Fig. 9 (b)). The laser treated fibers are totally consumed by diamond growth, because of much higher number density of diamond nuclei formed after laser annealing. In the case of untreated fibers, number density of diamond nuclei is considerably lower, as they are formed on the surface of fibers associated with strain centers and pits. The laser-treated fibers are totally consumed with a very high number density of diamond crystallites, as shown in Fig. 10 (a) at a higher magnification. Fig. 10 (b) shows the growth of diamond crystallites on the surface of untreated carbon fibers. These diamond crystallites merge and lead to formation of larger size crystallites. Both treated and untreated fibers show secondary nucleation of diamond crystallites. It should be mentioned that source for carbon in diamond growth is enhanced due to additional carbon containing species from the fibers. In the treated samples, nanodiamond nuclei formed after laser annealing provide a very effective nucleation sites. In untreated samples, diamond nucleation starts from the surface roughness at pits, which may provide strain centers for diamond nucleation and subsequent growth. It should be mentioned that there is hardly any diamond growth observed on pristine sapphire three-hour HFCVD growths. Fig 11 shows characteristic Raman spectra results from diamond after HFCVD growth from laser treated and untreated samples. The Raman peak at 1331.26 cm^{-1} is only slightly down shifted from the bulk diamond peak at 1332 cm^{-1} , indicating the presence of nanocrystalline diamond. The presence of G-peak at 1580 cm^{-1} (associated with graphitic carbon) is very weak for diamond growth in laser

treated fibers, characteristic of high-quality phase pure diamond. The G peak is more pronounced in untreated samples (CF-CVD-4F) due to the presence of unconsumed carbon fibers, compared laser-treated samples (CF-CVD-1S-4F).

The formation of DNFs starts with nucleation of diamond from the highly undercooled state of molten carbon (formed after PLA). The formation of diamonds occurs by a homogeneous nucleation from the highly undercooled state of carbon. The change in Gibbs free energy (ΔG_T) associated with the formation of DNFs consists of a gain in volume energy ($\sim r^3$) at the expense of surface energy ($\sim r^2$), where r is the radius of diamond nucleus. The change in free energy can be calculated using the equation: $\Delta G_T = \frac{-4}{3} \pi r^3 \frac{\rho}{M_m} \frac{\Delta H_m}{T_m} \Delta T_u + 4 \pi r^2 r_s$, where ρ is the density of diamond, ΔH_m is the latent heat of melting, M_m is the molar mass, and r_s is the surface free energy between diamond nuclei and the undercooled state of carbon. The first term in the equation is the volume energy term (gain in free energy for the formation of diamond nucleus from the undercooled state) whereas the second one is the surface energy term. The degree of undercooling, ΔT_u is equal to $T_m - T_r$, where T_m indicates melting point of graphite (~ 5000 K) and T_r indicates the nucleation temperature (~ 4000 K). With an increase in the value of ΔT_u , ΔG_T becomes more negative and a conversion of graphite (CNFs) to diamond (DNRs) is favorable. Again, the critical radius and change in Gibbs free energy (at $\frac{d\Delta G_T}{dr} = 0$) is inversely proportional to ΔT_u and ΔT_u^2 , respectively. Therefore increasing ΔT_u reduces the critical value of diamond radius and change in Gibbs free energy (ΔG_T^*). The rate of nucleation (I) is given by the equation: $I \sim \exp \frac{-\Delta G_T^*}{KT_r}$. Therefore, with a decrease in the value of ΔG_T^* , the rate of nucleation increases thereby facilitating the formation of diamond. For a 10 nm size nanodiamond, the estimated growth time is about 5-10 ns. This time requirement emphasizes the importance of

thermal conductivity of the substrate during rapid pulse laser heating. A rough estimate of r^* for diamond nuclei from equation is $\sim 20 \text{ \AA}$, where diamond surface free energy r_s is 0.6 Jm^{-2} , $T_m = 4000 \text{ K}$, $\Delta H_m = 1.0 \text{ eV/atom}$, $\Delta T_u = 1000 \text{ K}$, and $\rho = 3.5 \text{ gm/cm}^3$. This is verified experimentally in our earlier papers on diamond^{5,6} and on silicon.^{20,21,22} The growth velocity (v) is directly related to the undercooling by the following equation: $v = \frac{D_\infty f}{\lambda f_D} \left(1 - e^{-\frac{(T_m - T_u)\Delta S}{kT}} \right)$, where, D_∞ , f , λ , f_D , k , T , T_m , T_u and ΔS denote the liquid diffusivity ($\sim 10^{-8} \text{ m}^2/\text{sec}$ in liquid state), fraction of the available sites, atomic jump distance, geometrical factor associated with diffusion, Boltzmann constant, temperature, melting temperature, undercooling temperature, and the change in entropy, respectively. An increase in the value of T_u decreases the value of chemical free energy barrier for graphite to crystalline diamond phase transformation. This also increases the velocity of the melt-front. Therefore, the values of undercooling dictate the conversion of amorphous graphitic phase into diamond *via* the carbon melt. If the cooling rate is slow (low undercooling and low solidification velocity), crystalline graphite is formed whereas with high cooling rates (large undercooling and large solidification velocity), crystalline diamond is formed. We have synthesized diamond nanofibers from carbon nanofibers and carbon nanotubes by using a highly non-equilibrium technique of pulsed laser annealing. We have incorporated carbon nanofibers and carbon nanotubes on metallic substrates and irradiated with lasers to create highly efficient field emission devices. Upon irradiating the CNFs with nanosecond ArF laser, the tips and bends of the CNFs are melted in a highly undercooled state. The highly undercooled state of carbon is a metastable phase and nanodiamonds nucleate from this state. The process (rapid melting, solidification, and growth) is completed in less than 200 ns. Our results clearly indicate that diamond can be formed at ambient conditions in air from the super undercooled state of molten carbon without catalyst and atomic hydrogen (CVD process). The nanosecond laser parameters

and heat confinement by the one-dimensional CNFs determine the temperature distribution and undercooling and play a critical role in nucleation and growth of nanodiamonds. The nanosecond laser pulses help us to achieve the undercooled state of carbon and upon subsequent quenching leads to the formation of nanodiamonds from CNFs. The nanosecond laser heating and temperature distributions are confined spatially and temporally. Therefore, the tips (and bends) of CNFs melt whereas the underlying areas are unaffected. By subsequent laser pulses, these diamond regions can be extended to form larger diamond nanofibers and nanorods. The key consideration is undercooling, which depends upon thermal properties and heat flow geometry. By simulation of heat flow¹⁹ and taking into account of thermal properties for specific shapes, we can obtain laser parameters needed for the conversion into diamond. These nanorods and nanofibers can be doped with N and Si to create N-V and Si-V centers for quantum communication, quantum sensing and quantum computing. These nanostructures can be doped both *n*-type (such as N, P) and *p*-type (such as B) dopants for novel solid-state devices and high-efficiency field emitters. The formation of DNFs and their heterostructures will also have exciting applications ranging from drug delivery to optoelectronics and cellular sensors.²³ By controlling the nucleation and growth processes from the liquid, we can control formation of defects and create diamond structures with fewer undesirable defects. This is a very important consideration in diamond as defect annealing temperatures exceed 1700°C, above which high pressure is needed to stabilize diamond and anneal out defects. Such high temperatures and pressures needed for annealing defects in diamond render CVD grown diamonds not very useful for fabrication of solid-state devices.²⁴

4. Summary:

In our method, carbon nanotubes and carbon fibers are melted in a super undercooled state using high-power nanosecond laser pulses, and quenched rapidly to convert them into phase-pure diamond rods. The conversion process occurs at ambient temperature and pressure, and can be carried out in air. This process of conversion of carbon into diamond can be scaled by laser scanning, where 200 Hz laser can generate 200 cm² area per second. Our method leads to the formation of phase-pure diamond rods across the scale ranging from a few nanometers to micrometers and beyond depending upon initial size of carbon nanotubes and carbon fibers. The diamond-tipped carbon nanofibers and carbon nanotubes grown on metallic substrates provide ideal field emitters for next-generation contact-less energy-transfer systems and motors. This process can be scaled up to cover a large area over 100 to 200 cm² area per second using 100 to 200 Hz (repetition rate per second). These nanofibers can be doped selectively with *n*- and *p*-type dopants with concentrations far higher than thermodynamic solubility limits, by incorporating dopants before melting for a variety of potential applications ranging from quantum sensors to efficient catalysts and field emitters. The nano- and microdiamonds have been used very effectively as seeds to grow large diamonds by CVD methods for a variety of applications ranging abrasive powders for oil and gas exploration to diamond jewelry. This discovery of conversion of CNF tips into diamond nanofibers at room temperature and atmospheric pressure will open a new frontier for synthesis and processing of diamond nanostructures for a variety of applications, ranging from quantum computing, sensing and communication to field emission and tool coatings for oil and gas exploration and deep-sea drilling, in addition to diamond jewelry.

Acknowledgments:

We are grateful to Fan Family Foundation Distinguished Chair Endowment for Professor J. Narayan, and this research was funded by the National Science Foundation (DMR 1735695). We are also very pleased to acknowledge technical help and useful discussions with Professors Yuntian Zhu, John Prater and Roger Narayan.

References:

- 1 J. C. Angus and C. C. Hayman, *Science*, 1988, **241**, 913–21.
- 2 J. Narayan, V. P. Godbole and C. W. White, *Science*, 1991, **252**, 416–8.
- 3 F. P. BUNDY, H. T. HALL, H. M. STRONG and R. H. WENTORF, *Nature*, 1955, **176**, 51–55.
- 4 T. Irifune, A. Kurio, S. Sakamoto, T. Inoue and H. Sumiya, *Nature*, 2003, **421**, 599–600.
- 5 J. Narayan and A. Bhaumik, *J. Appl. Phys.*, 2015, **118**, 215303.
- 6 J. Narayan and A. Bhaumik, *APL Mater.*, 2015, **3**, 100702.
- 7 J. Narayan and A. Bhaumik, *APL Mater.*, 2016, **4**, 20701.
- 8 M. Pelliccione, A. Jenkins, P. Ovarthaiyapong, C. Reetz, E. Emmanouilidou, N. Ni and A. C. Bleszynski Jayich, *Nat. Nanotechnol.*, 2016, **11**, 700–705.
- 9 Y. Ando, Y. Nishibayashi and A. Sawabe, *Diam. Relat. Mater.*, 2004, **13**, 633–637.
- 10 L. T. Sun, J. L. Gong, D. Z. Zhu, Z. Y. Zhu and S. X. He, *Adv. Mater.*, 2004, **16**, 1849–1853.
- 11 C.-H. Hsu, S. G. Cloutier, S. Palefsky and J. Xu, *Nano Lett.*, 2010, **10**, 3272–3276.
- 12 B. Wei, J. Zhang, J. Liang and D. Wu, *Carbon N. Y.*, 1998, **36**, 997–1001.
- 13 C. Luo, X. Qi, C. Pan and W. Yang, *Sci. Rep.*, 2015, **5**, 13879.
- 14 F. Zhang, J. Shen, J. Sun, Y. Q. Zhu, G. Wang and G. McCartney, *Carbon N. Y.*, 2005, **43**,

- 1254–1258.
- 15 S. Ozden, L. D. Machado, C. Tiwary, P. A. S. Autreto, R. Vajtai, E. V. Barrera, D. S. Galvao and P. M. Ajayan, *ACS Appl. Mater. Interfaces*, 2016, **8**, 24819–24825.
- 16 W. K. Wang and L. M. Cao, *Russ. Phys. J.*, 2001, **44**, 178–182.
- 17 J. Zhang, R. Wang, X. Zhu, A. Pan, C. Han, X. Li, D. Dan Zhao, C. Ma, W. Wang, H. Su and C. Niu, *Nat. Commun.*, 2017, **8**, 683.
- 18 S. Praver and R. J. Nemanich, *Philos. Trans. R. Soc. London A Math. Phys. Eng. Sci.*
- 19 R. K. Singh and J. Narayan, *Mater. Sci. Eng. B*, 1989, **3**, 217–230.
- 20 J. Narayan and C. W. White, *Appl. Phys. Lett.*, 1984, **44**, 35–37.
- 21 J. Narayan, C. W. White, O. W. Holland and M. J. Aziz, *J. Appl. Phys.*, 1984, **56**, 1821.
- 22 R. F. Wood, D. H. Lowndes and J. Narayan, *Appl. Phys. Lett.*, 1984, **44**, 770.
- 23 R. Narayan, *Diamond-based materials for biomedical applications*, .
- 24 A. M. Zaitsev, *Proc. Natl. Acad. Sci.*, 2008, **105**, 17591–17592.

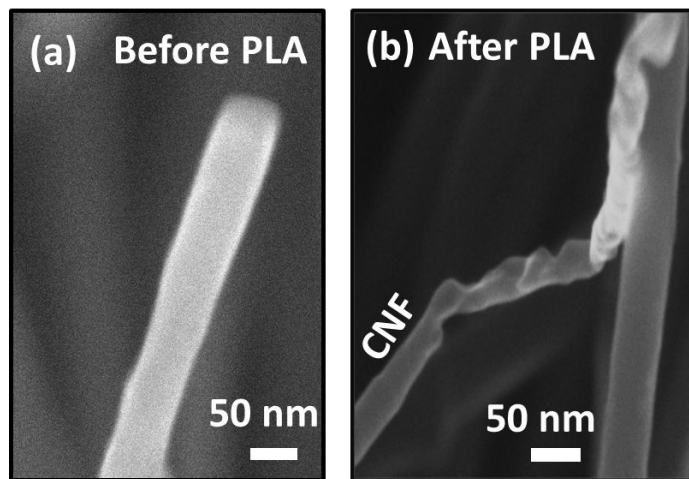
Figures:

Figure 1: High-resolution SEM images of (a) A CNF before PLA technique, (b) CNF after PLA showing the conversion carbon nanofibers into diamond nanofibers.

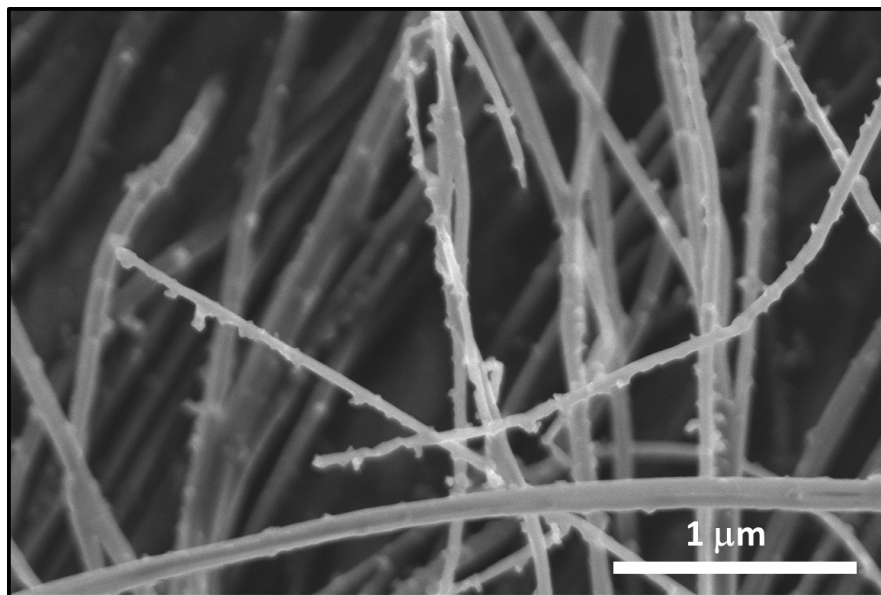


Figure 2: High-resolution SEM image showing conversion of carbon nanofibers of different diameters, where thin fibers are completely converted into diamond and thick fibers show diamond formation on the surface. Some of the surface nuclei grow into nanodiamond rods normal to the substrate along the diameter.

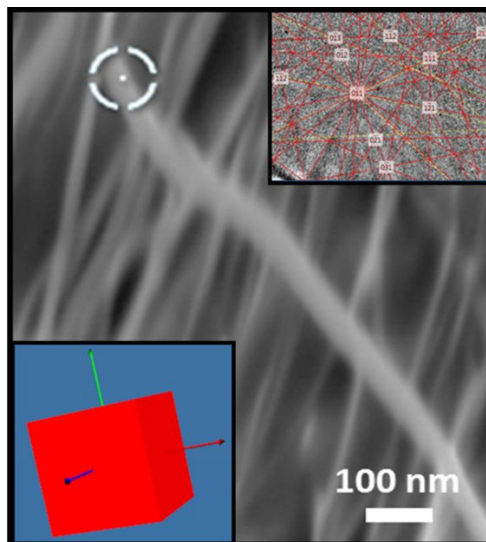


Figure 3: SEM micrograph of laser treated fibers with EBSD (Kikuchi) pattern characteristic of diamond and relative orientation (red cube) of diamond formed.

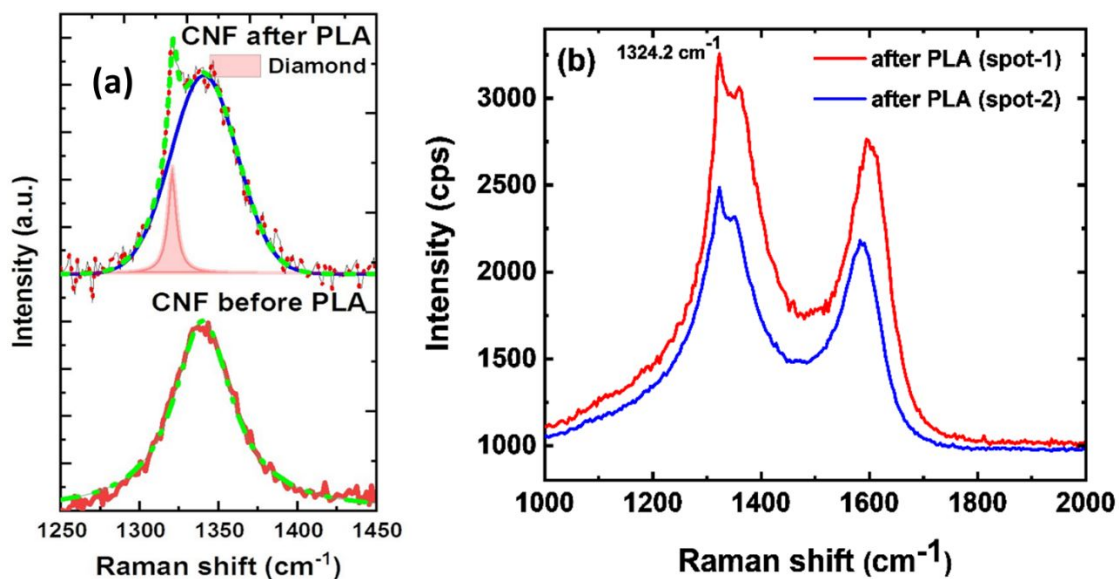


Figure 4: (a) Raman spectra before and after laser annealing in CNF, clearly showing diamond peak near 1321cm⁻¹, which downshifted from standard 1332 cm⁻¹ peak as result of phonon confinement, and (b) Raman spectra after PLA in CNT showing the sharp diamond peak at 1324.2 cm⁻¹.

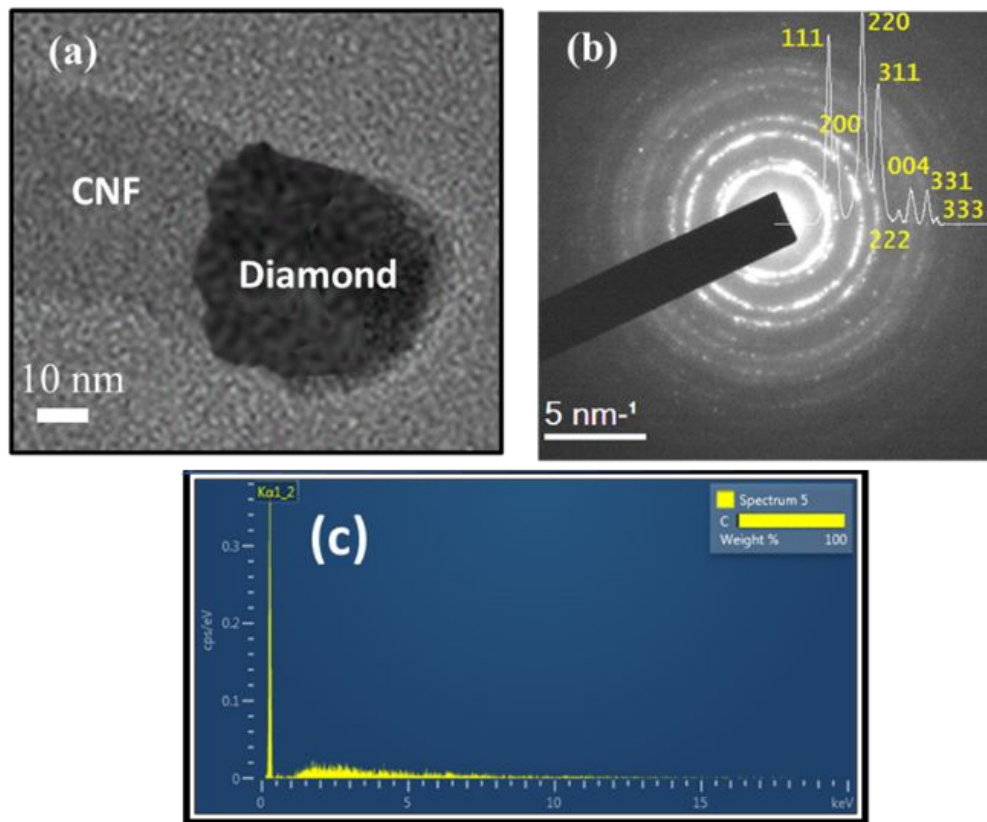


Figure 5: (a) TEM micrograph showing carbon nanofiber and diamond formation at the tip; (b) SAED pattern showing characteristic diamond diffraction rings, and (c) SEM-EDX of CNF after PLA.

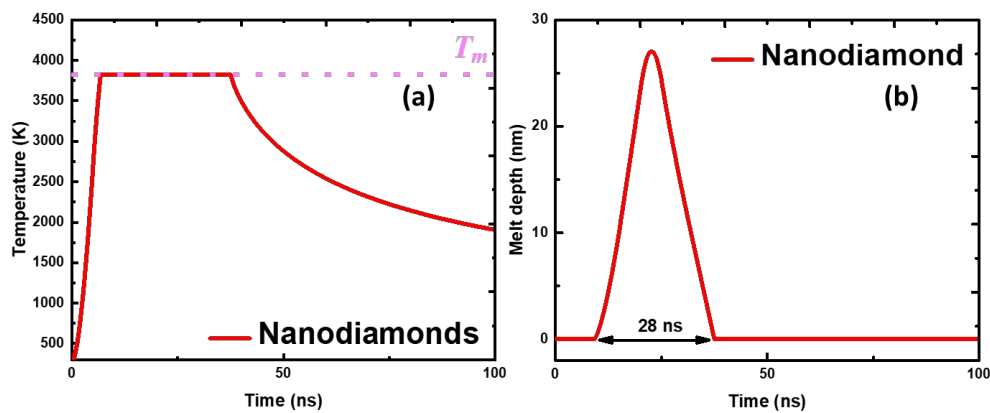


Figure 6: SLIM calculations using the following parameters: Melting temperature: 3823 K, Evaporation temperature: 5000 K, Latent heat of melting: 19775 J/cm³, Thermal conductivity of

solid: 3 W/mK, Thermal conductivity of molten carbon: 2.9 W/cmK, Absorption coefficient in solid state: $8.00e+05$, Absorption coefficient in liquid state: $1.00e+06$, Reflectivity in solid state: 0.3, Reflectivity in liquid state: 0.6, Annealing energy density: 0.6 J/cm², Laser pulse width: 20 ns.

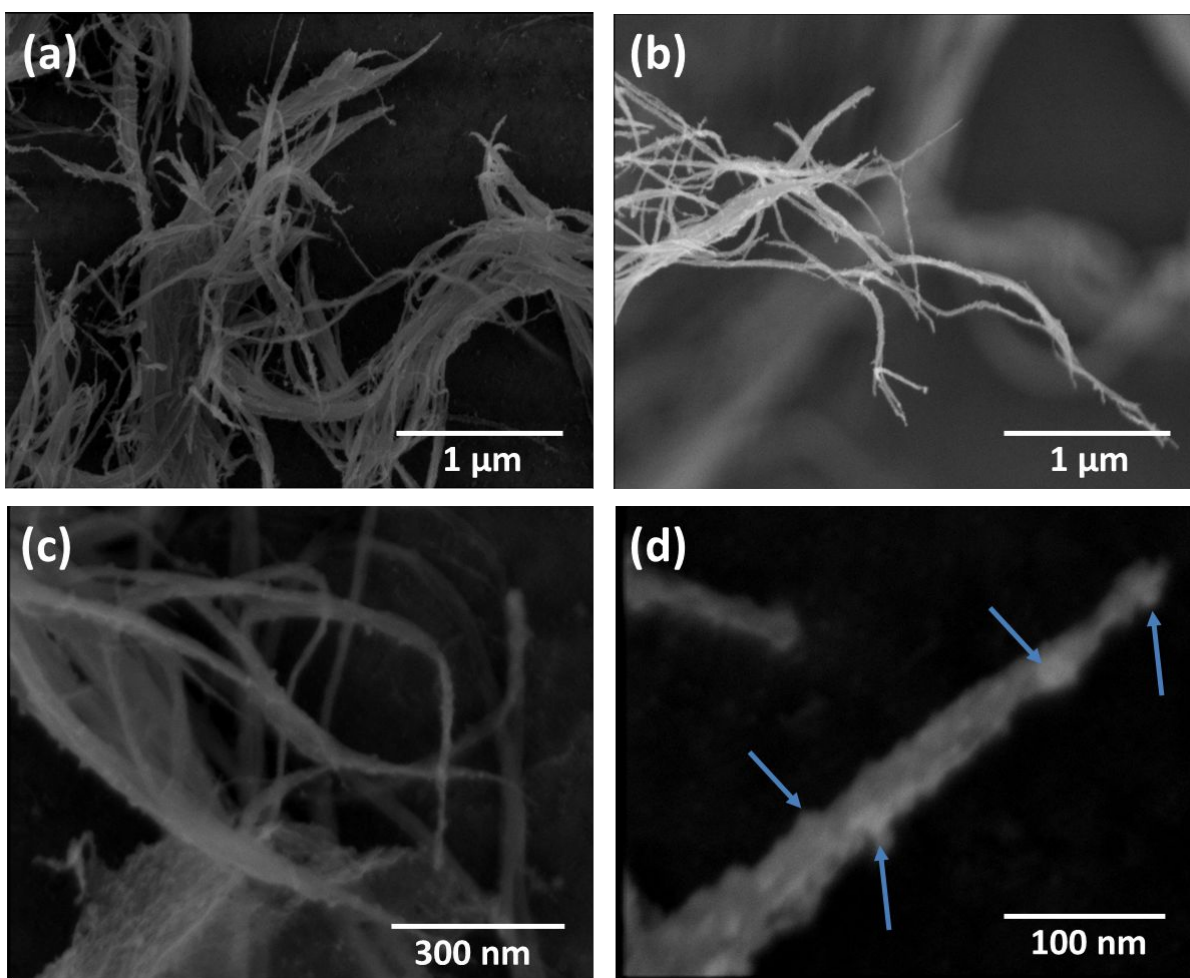


Figure 7: Conversion of carbon nanotubes into diamond nanorods; (a) SEM micrograph showing conversion of carbon nanotubes into diamond after 10 pulses of ArF laser (pulse duration 20ns) at 0.65 Jcm⁻²; (b) and (c) details of conversion process starting from the tips; and (d) nucleation of diamond in the middle of the nanotube and growth of diamond nanorods normal to the tube (shown by arrows).

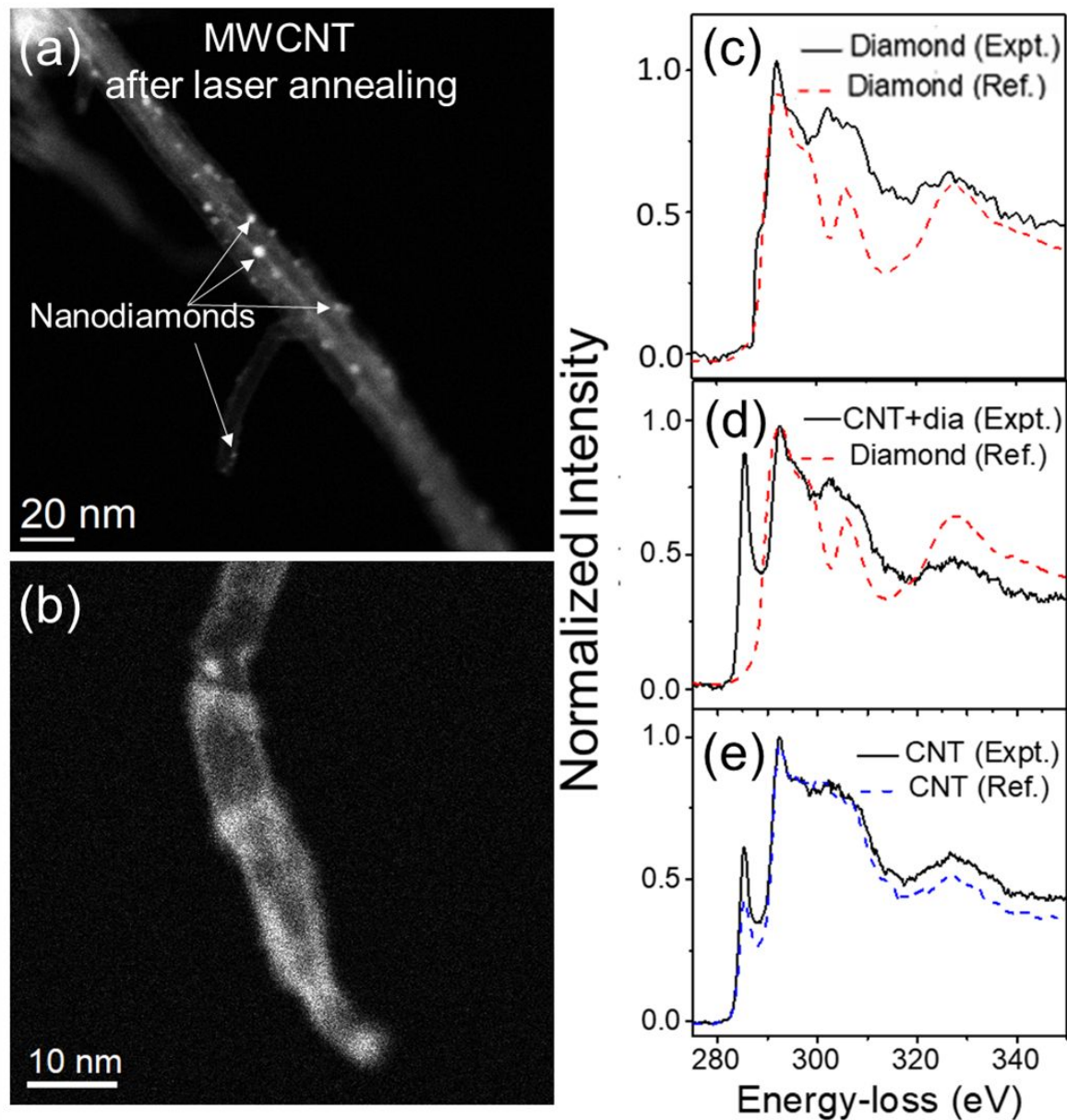


Figure 8: (a) HAADF image of CNTs after laser annealing showing the formation of nanodiamonds, (b) HAADF image of single CNT showing the formation of nanodiamonds at its edges and the end, EELS spectra of (c) diamond, (d) CNT and diamond obtained from the corresponding regions in laser annealed CNT, and (e) CNT before pulsed laser annealing. The reference spectra of diamond and CNT are also shown in figure (c) and (e), respectively for comparison.

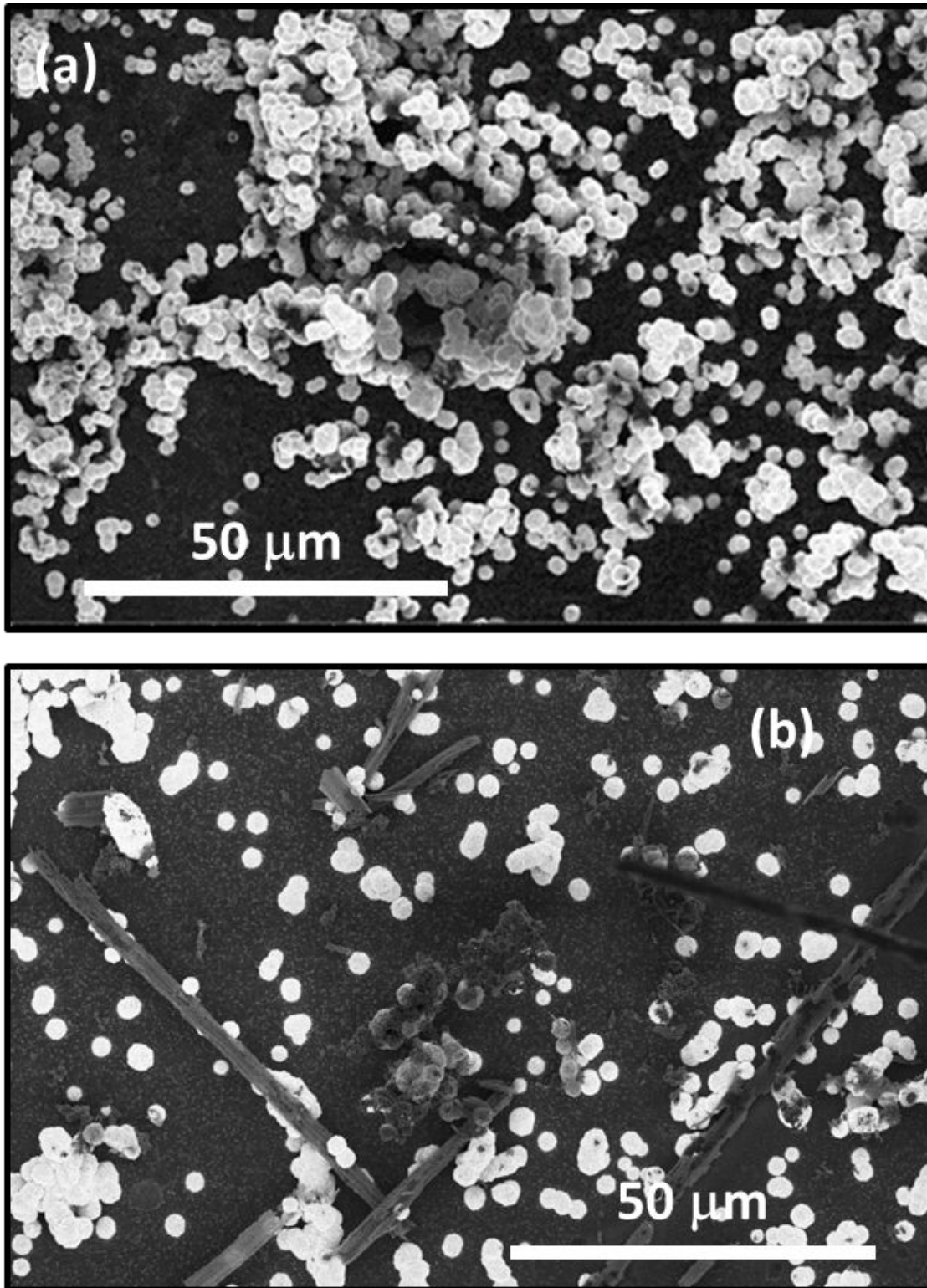


Figure 9: (a) HFCVD growth of diamond after laser annealing of carbon fibers (five microns diameter) with one pulse; and (b) HFCVD growth on untreated carbon fibers for a comparison.

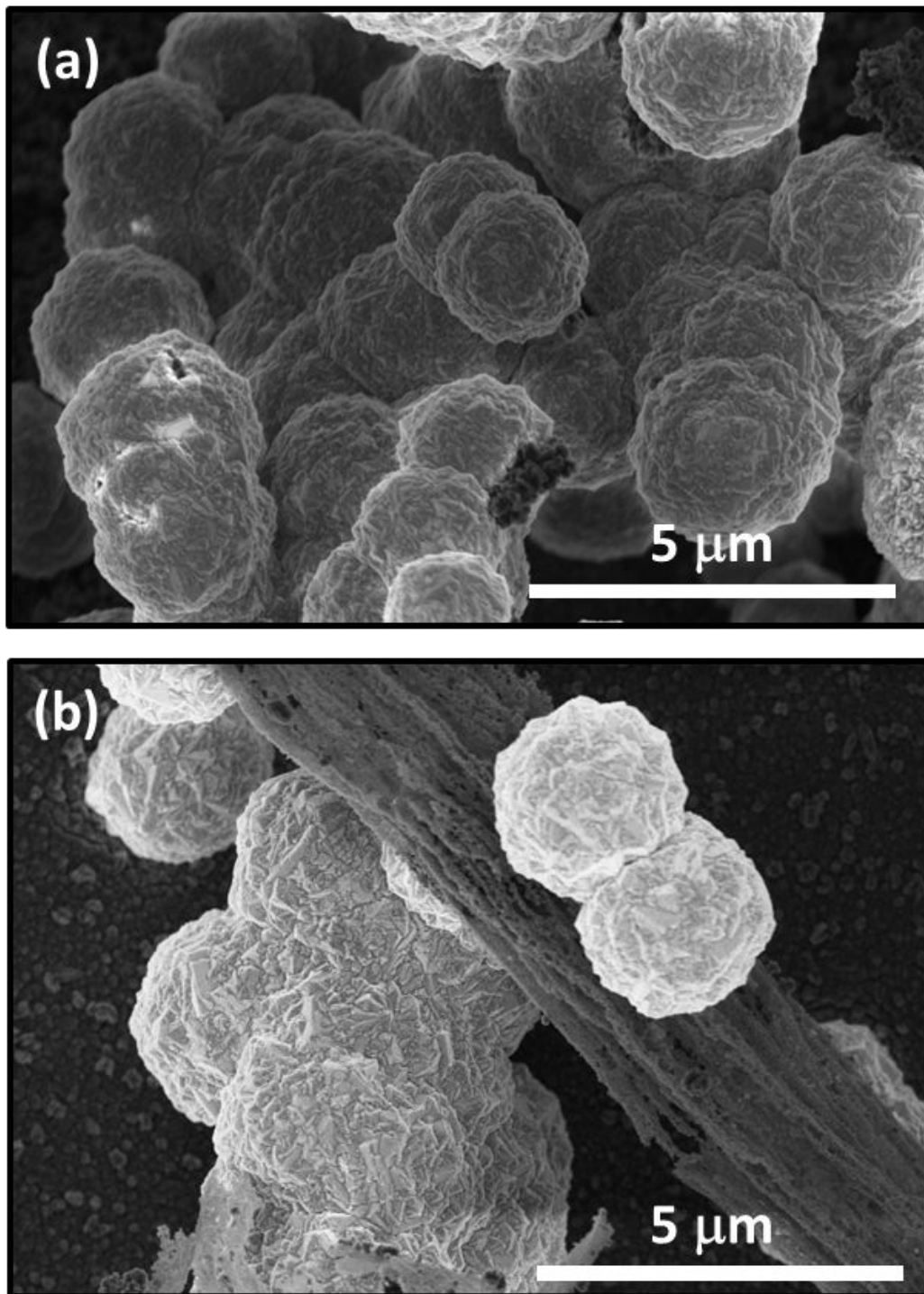


Figure 10: (a) Mechanism of HFCVD growth from laser treated fibers, showing multiple layers of diamond growth; and (b) Details of HFCVD growth of diamond on untreated fibers. Laser treated fibers provide much more effective sites for diamond growth during HFCVD.

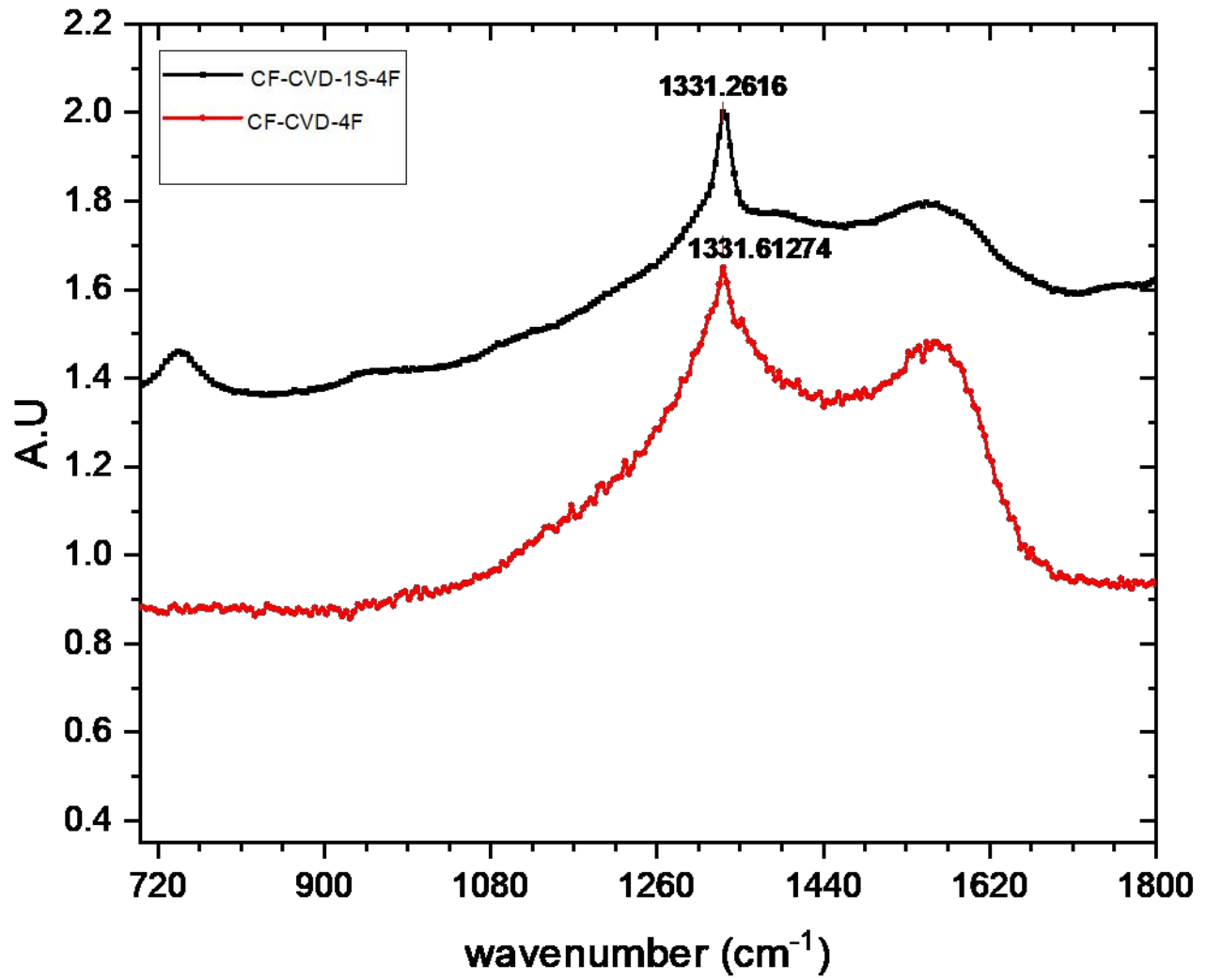
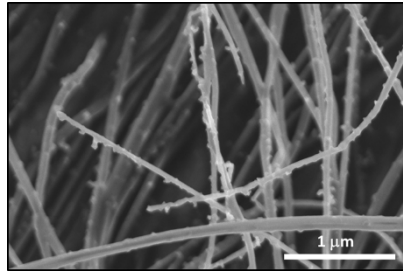


Figure 11: Characteristic Raman spectra from HFCVD grown diamond on treated and untreated carbon fibers, showing some graphitic peak in untreated samples.



We report a pulsed laser annealing method to convert carbon fibers and nanotubes into diamond fibers at ambient conditions.